Nanoparticles in a Capillary Trap: Dynamic Self-Assembly at Fluid Interfaces

Volodymyr Sashuk,[†,*] Katarzyna Winkler,[†] Andrzej Żywociński,[†] Tomasz Wojciechowski,[‡] Ewa Górecka,[§] and Marcin Fiałkowski[†,*]

[†]Institute of Physical Chemistry, Polish Academy of Sciences, Kasprzaka 44/52, 01-224 Warsaw, Poland, [‡]Institute of Physics, Polish Academy of Sciences, Al. Lotników 32/46, 02-668 Warsaw, Poland, and [§]Department of Chemistry, University of Warsaw, Żwirki i Wigury 101, 02-089 Warsaw, Poland

ABSTRACT Dynamic self-assembly is an emerging scientific concept aimed to construct artificial systems of adaptative behavior. Here, we present a first nanoscopic system that is able to dynamically self-assemble in two dimensions. This system is composed of charged gold nanoparticles, dispersed at the air–water interface, which self-assemble into a dense monolayer of area of several square centimeters in response to surface tension gradient. The surface tension gradient is imposed by localized addition or removal of organic solvent from the interface. After the surface tension is equalized over the whole fluid interface, the nanoparticles return to their initial dispersed state. The arrangement of nanoparticles before and after the self-assembly was characterized using SEM microscopy and SAXS spectroscopy. The constructed self-assembling system offers a "chemical" alternative for the Langmuir–Blodgett technique. Also, it was applied for creating self-erasing nanoparticle patterns on a fluid surface.

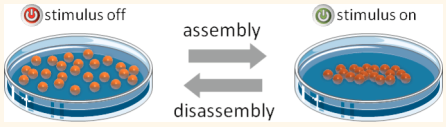

KEYWORDS: dynamic self-assembly · nanoparticles · interface · monolayer · surface tension

The concept of self-assembly (SA) is a main philosophy of current scientific research inspired by Nature.[1,2] This research is driven not only by scientific curiosity but also by a practical necessity. At the nanoscale, SA is the most feasible way to build large and complex structures from simple components such as nanoparticles (NPs).[3−5] However, the scientists are rarely able to mimic Nature, where the living entities function *via* dynamic self-assembly processes. In the man-made systems, the NPs are usually organized into complex, ordered assemblies whose structure does not change, in a process known as static SA.[6,7] Structures obtained in this way cannot be further modified or reconfigured because they correspond to the thermodynamic equilibrium of the system. In order to direct SA of NPs, the templates are commonly used.[8,9] One of the most popular templates is a fluid interface which facilitates SA of the NPs in two dimensions. Like most artificial self-assembled systems, all examples of ordering the NPs at the fluid interface reported in literature[10−18] belong to the class of static SA. Second class of the SA phenomena is dynamic SA (DySA) observed in steady-state systems brought away from equilibrium.[6,7,19−25] Formation of the ordered structures in such systems requires constant supply of energy, which is dissipated through entropy production. In contrast to static SA, DySA structures exhibit adaptative behavior and can reconfigure in response to external stimuli. As yet, the NP systems being able to self-assemble at fluid interfaces under non-equilibrium conditions have not been described. The development of such dynamic systems is of a paramount significance as it would lead to the fabrication of novel two-dimensional materials with adaptive properties. *Herein, we wish to report the first NP system that exhibits DySA at a fluid interface.* Our system consists of charged NPs uniformly dispersed at a gas–fluid interface. Creation of the gradient of the surface tension makes the NPs migrate toward the area of higher tension with formation of a dense monolayer. Spatial distribution of the surface tension is controlled by the presence of organic solvent over the fluid interface. The NP structures are present as long as the surface tension gradient is maintained. At equilibrium, when this gradient vanishes, the NPs return to their initial dispersed state.

Ⓦ This paper contains enhanced objects available on the Internet at http://pubs.acs.org/journals/ancac3.

* Address correspondence to vsashuk@ichf.edu.pl, mfialkowski@ichf.edu.pl.

Received for review June 28, 2013 and accepted September 2, 2013.

Published online September 02, 2013
10.1021/nn403297f

RESULTS AND DISCUSSION

Charged amphiphilic NPs represent an interesting class of nanocolloids. Amphiphilic NPs bearing a negative charge were found to exhibit an ability to penetrate and deliver a cargo into biological cells[28−33] and also to self-assemble at liquid interfaces[34] or incorporate into the wall of surfactant vesicles.[35] In the present study, we employed positively charged amphiphilic gold NPs recently developed in our group.[26,27] The ligand shell of the NPs was composed of a binary mixture of hydrophobic 1-undecanethiol (UDT) and hydrophilic 11-mercapto-*N*,*N*,*N*-trimethylundecane-1-aminium chloride/bromide (TMA) (Figure 1). The surface modification of the NPs was performed using 9:1 molar ratio of UDT/TMA. The mean size of the NP metal core was 8 nm. The experiments were carried out in the glass beakers filled with distilled water. Before use, the NPs were dispersed in the MeOH/DCM (1:4 v/v) mixture. Next, 30 μL of NP dispersion (4 mM in terms of gold) was dropped on the water surface of 11.34 cm^2 that corresponds theoretically to about 39% coverage of the NPs at the interface. Due to their amphiphilic structure and lateral electrostatic stabilization, the NPs were readily spread at the air−water interface to form uniform film of light-pink color.

The system composed of the amphiphilic NPs dispersed at the air−water interface exhibits DySA in response to external stimuli—gradient of the surface tension. We found that DySA of the interfacial NPs can occur in two different manners, referred to as DySA1 and DySA2. The difference between these two systems concerns the way in which the energy flux needed to maintain the emerging dynamic structures is dissipated. Both types of DySA are shown in Figure 1 (corresponding demonstrations are included as web-enhanced images video 1 and video 2 in the HTML).

In the DySA1 system (Figure 1b), one droplet (about 1 μL) of tetrahydrofuran (THF) was carefully placed on the water surface by a syringe near the rim of the experimental vessel. The addition of the solvent caused a spontaneous, rapid shrinking of the interfacial NPs into a compact, rigid film. Owing to changes in plasmonic response of the close-packed NPs, the film turned red-violet. This process was fully reversible. With time (typically, a couple of days), the sharp edges of the compressed NP monolayer smoothed and the dense film disintegrated to form a uniform layer. Thus, to sustain the DySA1 structure, a slow, but continuous, supply of the solvent on the interface was needed. This follows that the ordering of the NPs is maintained at the expense of the entropy production associated with the diffusion of the solvent into both the gas and liquid phases. The most remarkable feature of the DySA1 system is its huge asymmetry in the "on" and "off" response time to the external stimuli. That is, the system reacts instantly when the surface tension gradient is created (stimulus on) and relaxes slowly to the equilibrium state when it vanishes (stimulus off).

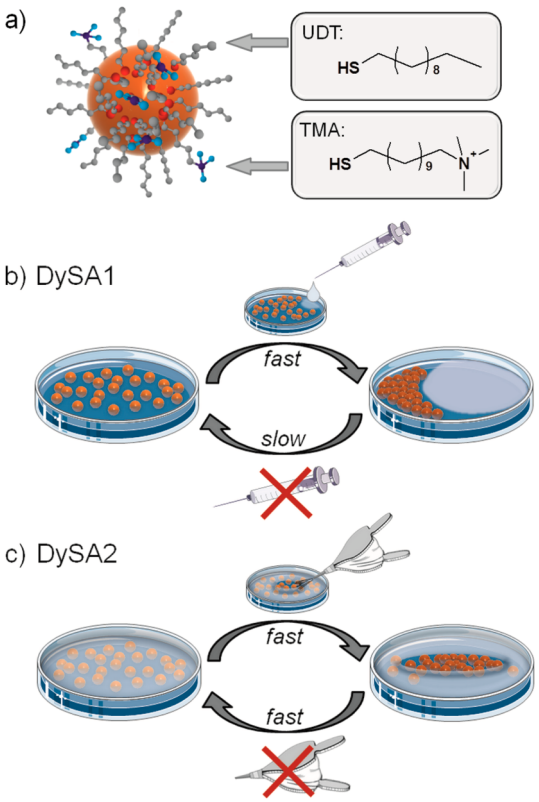

Figure 1. (a) Cartoon representation of the ligand shell of gold NP. (b,c) Illustration of dynamic self-assembly of the NPs at aqueous−air interfaces. Adding (b) or removing (c) solvent from the fluid interface creates the surface tension gradient, which makes the NPs compress into dense film. When the external stimulus is discontinued, the NPs disperse throughout the interface.

In the DySA2 (Figure 1c), the system was initially saturated by THF. The saturation was achieved in two different ways. In the first case, THF was gradually introduced by a syringe on the bottom of the experimental vessel until the content of the solvent in the aqueous phase reached approximately 50% (v/v). In order to provide the homogeneity of the liquid phase during the addition of the solvent, a continuous magnetic stirring was applied. In the second case, the beaker with the interfacial NPs was placed in a desiccator filled with THF. The degree of saturation of the system by THF required for DySA2 to occur was reached within 1 day. The sufficient content of THF in the aqueous phase was estimated as 5% (v/v). The system exhibited DySA2 property at such low solvent content because, upon saturation of the system by solvent vapors, THF, which has a density smaller than that of water, is concentrated in the upper layer of the aqueous phase and saturates quickly in the gas phase above the interface. The system starts working when the air flow is directed toward the interface. The NPs organize instantly into a dense film at the place from which the air saturated with vapors of the organic solvent was blown out. When the air supply ceases, the compressed NP film disintegrates into a sparse

monolayer within a few seconds. The cycles of NP compression–decompression can be repeated, at least, for a dozen times. In DySA2, the ordered structure is maintained by the steady flux of kinetic energy of the air jet reaching the interface. Compared with the DySA1 system, DySA2 is characterized by relatively small asymmetry in the "on" and "off" response times.

The arrangement of the NPs, before and after the compression, was first studied by the scanning electron microscopy (SEM). The characterization of interfacial NP structures was possible only for the DySA1 system where the time-span between assembly and disassembly events is large. The interfacial NPs were cast onto a solid substrate by immersing a silicon wafer into the subphase and, next, pulling it away under an angle of about 20° relative to the plane of the interface. The corresponding SEM images are presented in Figure 2. The SEM analysis revealed that, upon treatment with THF, the NPs were compressed into a compact, densely packed monolayer. Interestingly, the NPs collected from the sparse film were also arranged into close-packed domains, but these domains were small and evenly distributed throughout the surface. To ensure that the NP ordering, observed in the SEM images, corresponds to that at the fluid interface, we performed *in situ* SAXS measurements. The SAXS technique allowed us to study the NP arrangement directly at the air–water interface, thereby eliminating any effects that might occur during the deposition and drying of the NP film on the solid substrate. The obtained X-ray scattering patterns along with the corresponding integrated spectra are presented in Figure 2. In both cases, the peaks were located at 11.02 nm. This value corresponds closely to the calculated diameter of the single NP. The thickness of the NP ligand shell is approximated by the length of the UDT ligand (1.57 nm). The diameter of the NP is calculated as $8 + (2 \times 1.57)$ nm = 11.14 nm. This result indicated that the NPs, both before and after the compression, are arranged close to each other at the interface. However, based on the SAXS data, it is hard to determine the characteristic size of the NP domain. While the formation of the large-area NP monolayer after compression is implicitly evidenced by visual observation and further corroborated by SEM analysis, the exact arrangement of the NPs at the interface before the compression remained unknown. Probably, there is a certain equilibrium between separated and grouped NPs at the interface that results from a delicate balance between hydrophobic and electrostatic interactions of the NP ligand shells. This equilibrium depends also on the surface concentration of the interfacial NPs. Importantly, due to the aforementioned force balance, the ligand chains of the neighboring NPs do not interdigitate much, as it follows from the comparison of the calculated and measured interparticle distance values. We believe that the lack of strong irreversible interactions between the interfacial NPs enables the system to dynamically self-assemble.

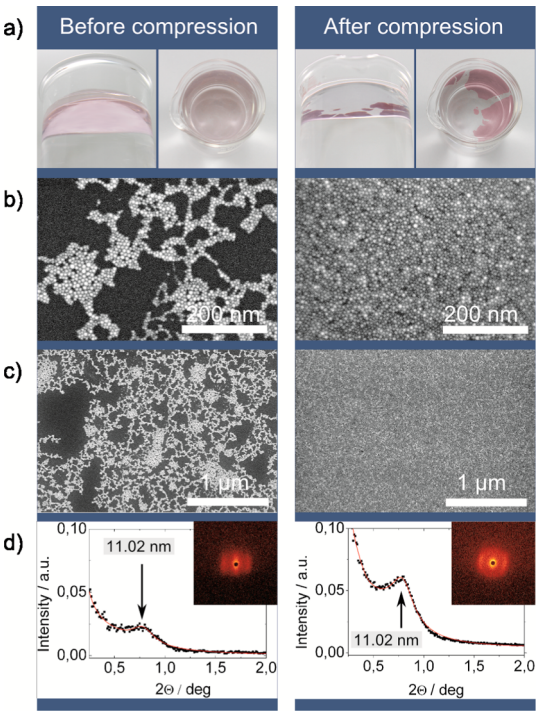

Figure 2. Representations of NPs before and after the compression in the DySA1 system: (a) digital photos of the experiment; (b,c) SEM images at high and low magnification, respectively; (d) SAXS patterns and integrated spectra.

The mechanism of DySA of the NPs at the fluid interface is inherently capillary. By adding or removing the volatile organic solvent from the interface, the surface tension gradient is created. Due to the imbalance of the capillary forces, the interfacial NPs move in the direction of higher surface tension (see Figure 3). When the surface tension is equilibrated, the NPs again scatter at the interface. Importantly, the surface tension gradient is not created when the solvent is uniformly introduced into the system, as in the case of saturation of the DySA2 system with THF. In the case of DySA1, the reverse process is slow due to attractive hydrophobic interactions between the aliphatic chains of the compressed NPs. This is the reason for the huge differences in the "on" and "off" reaction time to the stimuli observed in DySA1. Note that when hydrocarbon solvent (*e.g.*, pentane, hexane, or toluene) was put on the compressed layer of the NPs, the hydrophobic interactions significantly weakened and the NPs quickly spread at the interface. Likewise, the gaseous THF disperses the interfacial NPs during the reverse process in the DySA2 system. When the air blowing was stopped, the THF vapors filled instantly the entire interface, causing the NPs to disassemble.

From the above discussion, it follows that, in both DySA1 and DySA2 systems, the same "capillary trap" mechanism is responsible for the NP assembling. However, this mechanism is operating in an "opposite" way in these two cases: In DySA1, the surface tension

gradient is imposed by adding organic solvent at the air–aqueous interface. The surface tension between the air and the THF-rich aqueous phase is lower than that between the air and pure water. In DySA2, the gradient is formed by removing THF from above the interface. The surface tension between the THF-rich air and the THF-rich aqueous phase is lower than that between the air containing no THF and the THF-rich aqueous phase.

Our results indicate that the solvents with lower surface tension values (γ) should be most efficient for DySA. However, we found that the ability of the solvent to create the surface tension gradient depends on its relative miscibility with water. This ability can be correlated with the Hildebrand solubility parameter.[36] The efficiency of each solvent, assessed based on a visual observation of the amount of solvent needed to compress the NPs, and its correlation with solubility parameter are presented in Table 1. As can be seen, the most efficient solvent, THF, has the lowest solubility parameter among all water-miscible solvents. The relationship between the solubility parameter of the solvent and its ability to create the surface tension gradient was proved also experimentally. We found that the addition of 10 μL of THF (γ = 26.70 mN/m)[37] at the air–water interface of 30 cm^2 produces an abrupt change of the surface tension of 4.93 mN/m. On the other hand, in a similar experiment with acetone (γ = 22.72 mN/m)[37] and methanol (γ = 22.07 mN/m),[37]

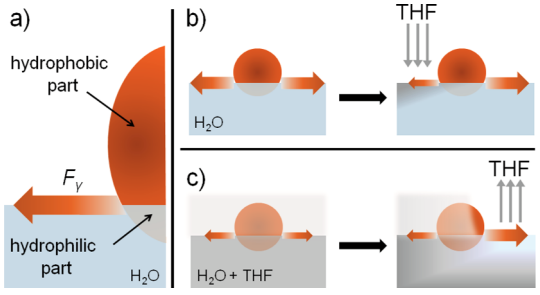

Figure 3. "Capillary trap" mechanism underlying dynamic self-assembly of the NPs. Upper and lower images (left b and c) represent the NPs located at the air–liquid interfaces of pure water and the aqueous phase saturated with THF, respectively. The capillary forces (red arrows, F_γ) acting on the NP depend on the surface tension (a) and are balanced (left b and c) when the fluid phases are homogeneous. When the NP experiences a gradient of the surface tension (caused by adding or removing THF), the resultant force pulls the NP toward the area of higher surface tension.

the surface tension decreases by 1.84 and 1.22 mN/m, respectively. The assumption that the compression of the NPs at the interface results from the surface tension gradient was confirmed in the experiments with conventional surfactants. It is well-known that micro- and even macroparticles are capable of moving on liquid interfaces in response to surface tension gradient created by addition of surfactant.[38,39] This phenomenon is often used in popular science demonstrations with ground pepper and dish soap. A grain of any surfactant (cationic CTAB, anionic SDS, or neutral $C_{12}E_{10}$) put at the air–water interface also caused instant compression of the interfacial NPs into a dense film. However, in contrast to DySA1, this process was irreversible (not dynamic) because the surfactant remained on the interface. As in the case of solvents, among the three surfactants studied, the least soluble one (*i.e.* $C_{12}E_{10}$) exhibited the best compression efficiency.

One could conjecture that the compression of the NPs might be induced by the electrostatic screening. We noticed that the solvents' efficiency, presented in Table 1, correlates nicely with dielectric constants, where THF—the most efficient solvent—displays the lowest dielectric constant. To check whether the electrostatic mechanism is operable, we decided to lower the dielectric constant of the aqueous phase by alternative approach, namely, by increasing the ionic strength of the medium through the addition of inorganic salt (NaCl). However, we found that the decrease of the permittivity of the aqueous phase does not result in the compression of the NPs as it was in the case of solvents. In the high salt concentrations (higher than 2 M), the interfacial NPs aggregated and then sintered into larger particulates (see Supporting Information).

Finally, we checked whether the solvent-induced compression mechanism is operable in the case of uncharged NPs. In our study, we employed the NPs coated with the UDT ligand shell. We found that the addition of THF leads also to the compression of the NPs. This finding ultimately confirms that the compression is driven by the capillary forces and rules out the effect of the electrostatic screening. In contrary to the charged NPs, the uncharged NPs were found to bunch instantly into rafts once placed at the air–water interface due to strong hydrophobic interactions. After the solvent was added, these rafts aggregated into a large single domain. Such obtained NP film contained many multilayers and voids due to the inability of the system

TABLE 1. Correlation of Solvent Efficiency with Solubility Parameters and Dielectric Constants

solvents	THF	acetone	isopropyl alcohol	DMF	ethanol	methanol	DMSO	water
observed efficiency	very high (<1 μL)	high (>1 μL)		medium (>10 μL)			no effect	
solubility parameter[a] (MPa$^{1/2}$)	19.0	19.6	23.6	23.8	26.1	29.3	26.7	47.8
dielectric constant	7.5	21.0	20.2	38.3	25.3	33.0	47.2	80.1

[a] Calculated according to ref 8 using the values of enthalpy of evaporation and molar volume at T = 298.2 K from ref 9. Approximate amounts of solvents required for compression of the NPs (30 μL of NP dispersion dropped on the water surface of 11.34 cm^2) into a rigid film are given in parentheses.

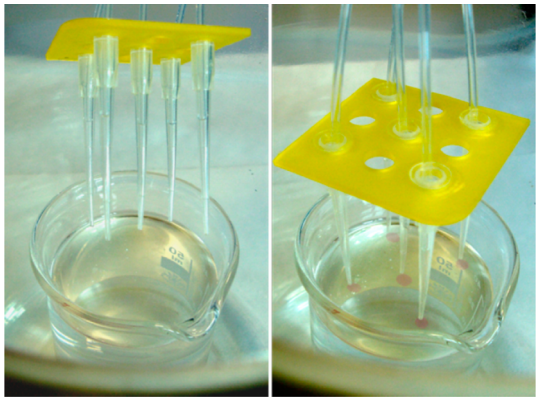

Figure 4. Making self-erasing NP patterns using the DySA2 system. Left image shows the NP monolayer (not visible by the naked eye) on the aqueous surface without air blowing. Right image shows the NP pattern (red spots) formed upon air blowing from five plastic nozzles.

to fit the NP rafts during the assembly process. The strong interactions of the hydrophobic NPs at the interface hamper their separation, making the assembly process irreversible and, hence, nondynamic.

The designed self-assembling systems have a great application potential. As we show, the DySA1 system offers a facile tool to fabricate NP monolayers. Our preliminary studies demonstrated also the possibility to harness the dynamic nature of the DySA2 system to control the spatial distribution of NP assemblies on fluid interfaces. After slight modification of the DySA2 experimental setup, we were able to create simple geometrical self-erasing patterns (Figure 4): For preparation of the NP monolayer, 8 μL of NP dispersion (4 mM in terms of gold) was dropped on the water surface of 11.34 cm^2 that corresponds theoretically to about 10% coverage of the NPs at the interface. Next, the system was saturated with THF vapors for 1 day. The air flow blown simultaneously from five nozzles produced a pattern resembling a five-pips die face, which disappeared once the air supply stopped. The cycle of writing–erasing of the pattern could be repeated at least a dozen times. As a part of future work, we expect that by changing the arrangement, shapes, and sizes of the nozzle apertures' distance between the nozzles and the interface, as well as by tuning the NP concentration and the air flow intensity it would be possible to create more complex patterns of prescribed geometry.

CONCLUSIONS

In summary, we constructed a system composed of charged NPs which are able to dynamically self-assemble at the gas–liquid interface. In response to the external stimulus—creation of the gradient of the surface tension—the NPs migrate to the regions of higher surface tension. That is, the NPs get into the *capillary trap*. The surface tension gradient is created by applying THF. When the surface tension gradient vanishes, the NP assemblies spontaneously disassemble. The designed DySA system can work in two different modes: either by introducing THF (DySA1) or by removing it from the interface (DySA2). These two systems differ in the way the energy flux needed to sustain the dynamic structures is supplied and dissipated. The engineering of both the DySA systems was possible thanks to the rational design of the NP ligand shell that stabilizes the NPs at the gas–liquid interface. DySA1, caused by the addition of the THF, can be considered as a chemical analogue of the Langmuir–Blodgett (LB) technique and, therefore, can be employed for the fabrication of the large-area NP monolayer films which have aroused recently great practical interest as a potential component for novel devices and materials.[40–45] In contrast to the LB technique, our method of the NP film fabrication is very simple, fast, and can be performed in any lab with no need to apply specialized and cumbersome equipment. The fast-responding version of the NP self-assembly, that is, DySA2, was successfully applied for creation of self-erasing NP patterns at the gas–liquid interface. It also can be considered as a prototype of an adaptive plasmonic system, which responds to the environmental changes of the surface tension.

EXPERIMENTAL SECTION

Materials and Instrumentation. Chemicals and materials were purchased as reagent grade from commercial suppliers and used without further purification: dodecylamine (DDA), 1-undecanethiol (UDT), gold(III) chloride trihydrate, 11-bromo-1-undecene, and thioacetic acid from Sigma-Aldrich, 33% w/w solution of trimethylamine in EtOH (Alfa-Aesar), 1.25 M solution of HCl in MeOH and AIBN from Fluka, analytically pure solvents (ChemPur, POCh), silicon wafers (Cemat Silicon SA). 11-Mercapto-*N*,*N*,*N*-trimethylundecane-1-aminium chloride/bromide (TMA) was prepared in three steps by adopting literature procedures:[46,47] (a) quaternization of 11-bromo-1-undecene with trimethylamine in ethanol; (b) radical addition of thioacetic acid to double bond; (c) deprotection of thiol (removing acetyl group) using HCl/MeOH. The EDS analysis of resulting TMA powder showed that the product contains, besides the chloride anion, also a bromide anion in quantities of about 20–30%. DDA-capped gold NPs were prepared according to the literature procedure.[48] In all experiments, Milli-Q water (18 MΩ·cm) was used.

SEM imaging and EDS analysis were performed using Neon 40-Auriga Zeiss scanning electron microscopy. The small-angle X-ray scattering (SAXS) spectra were obtained with the Bruker Nanostar system, and the patterns were registered with the Vantec 2000 area detector; Cu Kα (α =1.54 Å) radiation was used. The size of the NP metal core was estimated based on SAXS measurements. The surface tension measurements were conducted using the equipment from Nima Technology: a 50 × 750 × 10 mm Teflon trough was equipped with two barriers for symmetric compression and a film balance 0.01 mN/m resolution.

Preparation of Charged NPs. The DDA-capped Au NPs (0.04 mmol in terms of gold atoms) were first precipitated by adding methanol (20 mL) in order to remove an excess of surfactant and amine. The supernatant liquid over precipitated NPs was then carefully decanted. Next, the NP precipitate was dispersed in 5 mL of chloroform and injected into a stirred solution of TMA

and UDT mixture in a 1:9 ratio (total amount of ligands was 0.04 mmol) in chloroform (5 mL). The reaction mixture was left stirring overnight. Thiol-coated NPs collected by centrifugation (4000−6000 rpm, 5 min) were next purified by utilizing a dissolution−precipitation protocol. The NPs were dissolved in methanol (1.5 mL) followed with addition of 1.5 mL of isopropyl alcohol and precipitated with *n*-hexane (40−50 mL). The precipitated NPs were centrifuged at 4000−6000 rpm for 5 min. The dissolution−precipitation cycle was repeated 5−7 times. Finally, the purified, thiol-coated gold NPs were dried and dissolved in 2 mL of methanol to give 20 mM NP dispersion. Before use in the SA experiments, the NP dispersion was diluted with dichloromethane to give 4 mM dispersion.

Preparation of Uncharged NPs. The DDA-capped Au NPs (0.04 mmol in terms of gold atoms) were first precipitated by adding methanol (20 mL) in order to remove an excess of surfactant and amine. The supernatant liquid over precipitated NPs was then carefully decanted. Next, the NP precipitate was dispersed in 5 mL of chloroform, and UDT ligand (0.04 mmol) was injected into the stirred NP dispersion. The reaction mixture was left stirring overnight. Thiol-coated NPs were precipitated using methanol and collected by centrifugation (4000−6000 rpm, 5 min). Next, the NP precipitate was purified by utilizing the dissolution−precipitation protocol. The NPs were dissolved in *n*-hexane (1 mL) and precipitated with methanol (40−50 mL). The precipitated NPs were centrifuged at 4000−6000 rpm for 5 min. The dissolution−precipitation cycle was repeated 5−7 times. Finally, the purified, thiol-coated gold NPs were dried and dissolved in 2 mL of chloroform to give a 20 mM NP dispersion. Before use in the SA experiments, the NP dispersion was diluted with chloroform to give a 4 mM dispersion.

Conflict of Interest: The authors declare no competing financial interest.

Web Enhanced. Video demonstrations of DySA processes are available in the HTML version of the paper.

Acknowledgment. This work was financed by Ministry of Science and Higher Education of Poland in frame of grant Iuventus Plus IP2011 048271. Financial support from the National Science Centre (Grant 2011/01/N/ST5/02916) and the Foundation for Polish Science Team Programme cofinanced by the EU "European Regional Development Fund" Grant No. TEAM/2010-6/4 is also acknowledged.

Supporting Information Available: Estimation of NP coverage, figures showing the abrupt change of surface tension after adding solvents, setup for making self-erasing NP patterns, SEM images representing the NP structures formed at the air−water interface after adding salt and surfactants. This material is available free of charge *via* the Internet at http://pubs.acs.org.

REFERENCES AND NOTES

1. Whitesides, G. M.; Grzybowski, B. Self-Assembly at All Scales. *Science* **2002**, *295*, 2418–2421.
2. Lehn, J.-M. Toward Self-Organization and Complex Matter. *Science* **2002**, *295*, 2400–2403.
3. Bishop, K. J. M.; Wilmer, C. E.; Soh, S.; Grzybowski, B. A. Nanoscale Forces and Their Uses in Self-Assembly. *Small* **2009**, *5*, 1600–1630.
4. Nie, Z.; Petukhova, A.; Kumacheva, E. Properties and Emerging Applications of Self-Assembled Structures Made from Inorganic Nanoparticles. *Nat. Nanotechnol.* **2010**, *5*, 15–25.
5. Min, Y.; Akbulut, M.; Kristiansen, K.; Golan, Y.; Israelachvili, J. The Role of Interparticle and External Forces in Nanoparticle Assembly. *Nat. Mater.* **2008**, *7*, 527–538.
6. Mann, S. Self-Assembly and Transformation of Hybrid Nano-objects and Nanostructures under Equilibrium and Non-equilibrium Conditions. *Nat. Mater.* **2009**, *8*, 781–792.
7. Grzybowski, B. A.; Wilmer, C. E.; Kim, J.; Browne, K. P.; Bishop, K. J. M. Self-Assembly: From Crystals to Cells. *Soft Matter* **2009**, *5*, 1110–1128.
8. Grzelczak, M.; Vermant, J.; Furst, E. M.; Liz-Marzán, L. M. Directed Self-Assembly of Nanoparticles. *ACS Nano* **2010**, *4*, 3591–3605.
9. Shenhar, R.; Norsten, T. B.; Rotello, V. M. Polymer-Mediated Nanoparticle Assembly: Structural Control and Applications. *Adv. Mater.* **2005**, *17*, 657–669.
10. Böker, A.; He, J.; Emrick, T.; Russell, T. P. Self-Assembly of Nanoparticles at Interfaces. *Soft Matter* **2007**, *3*, 1231–1248.
11. Niu, Z.; He, J.; Russell, T. P.; Wang, Q. Synthesis of Nano/Microstructures at Fluid Interfaces. *Angew. Chem., Int. Ed.* **2010**, *49*, 10052–10066.
12. Ma, H.; Hao, J. Ordered Patterns and Structures *via* Interfacial Self-Assembly: Superlattices, Honeycomb Structures and Coffee Rings. *Chem. Soc. Rev.* **2011**, *40*, 5457–5471.
13. Kinge, S.; Crego-Calama, M.; Reinhoudt, D. N. Self-Assembling Nanoparticles at Surfaces and Interfaces. *ChemPhysChem* **2008**, *9*, 20–42.
14. Popp, N.; Kutuzov, S.; Böker, A. Various Aspects of the Interfacial Self-Assembly of Nanoparticles. In *Complex Macromolecular Systems II*; Müller, A. H. E., Schmidt, H.-W., Eds.; Springer: Berlin, 2010; Vol. 228, pp 39−58.
15. Garbin, V.; Crocker, J. C.; Stebe, K. J. Nanoparticles at Fluid Interfaces: Exploiting Capping Ligands To Control Adsorption, Stability and Dynamics. *J. Colloid Interface Sci.* **2012**, *387*, 1–11.
16. McGorty, R.; Fung, J.; Kaz, D.; Manoharan, V. N. Colloidal Self-Assembly at an Interface. *Mater. Today* **2010**, *13*, 34–42.
17. Wang, J.; Wang, D.; Sobal, N. S.; Giersig, M.; Jiang, M.; Möhwald, H. Stepwise Directing of Nanocrystals To Self-Assemble at Water/Oil Interfaces. *Angew. Chem., Int. Ed.* **2006**, *45*, 7963–7966.
18. Duan, H.; Wang, D.; Kurth, D. G.; Möhwald, H. Directing Self-Assembly of Nanoparticles at Water/Oil Interfaces. *Angew. Chem., Int. Ed.* **2004**, *43*, 5639–5642.
19. Grzybowski, B. A.; Campbell, C. J. Complexity and Dynamic Self-Assembly. *Chem. Eng. Sci.* **2004**, *59*, 1667–1676.
20. Fialkowski, M.; Bishop, K. J. M.; Klajn, R.; Smoukov, S. K.; Campbell, C. J.; Grzybowski, B. A. Principles and Implementations of Dissipative (Dynamic) Self-Assembly. *J. Phys. Chem. B* **2006**, *110*, 2482–2496.
21. Wang, L.; Xu, L.; Kuang, H.; Xu, C.; Kotov, N. A. Dynamic Nanoparticle Assemblies. *Acc. Chem. Res.* **2012**, *45*, 1916–1926.
22. Jha, P. K.; Kuzovkov, V.; Grzybowski, B. A.; Olvera de la Cruz, M. Dynamic Self-Assembly of Photo-switchable Nanoparticles. *Soft Matter* **2012**, *8*, 227–234.
23. Chen, Y.; Shi, Y. Dynamic Self Assembly of Confined Active Nanoparticles. *Chem. Phys. Lett.* **2013**, *557*, 76–79.
24. Chovnik, O.; Balgley, R.; Goldman, J. R.; Klajn, R. Dynamically Self-Assembling Carriers Enable Guiding of Diamagnetic Particles by Weak Magnets. *J. Am. Chem. Soc.* **2012**, *134*, 19564–19567.
25. Li, L.; Köpf, M. H.; Gurevich, S. V.; Friedrich, R.; Chi, L. Structure Formation by Dynamic Self-Assembly. *Small* **2012**, *8*, 488–503.
26. Sashuk, V.; Hołyst, R.; Wojciechowski, T.; Górecka, E.; Fiałkowski, M. Autonomous Self-Assembly of Ionic Nanoparticles into Hexagonally Close-Packed Lattices at a Planar Oil−Water Interface. *Chem.—Eur. J.* **2012**, *18*, 2235–2238.
27. Sashuk, V.; Hołyst, R.; Wojciechowski, T.; Fiałkowski, M. Close-Packed Monolayers of Charged Janus-Type Nanoparticles at the Air−Water Interface. *J. Colloid Interface Sci.* **2012**, *375*, 180–186.
28. Uzun, O.; Hu, Y.; Verma, A.; Chen, S.; Centrone, A.; Stellacci, F. Water-Soluble Amphiphilic Gold Nanoparticles with Structured Ligand Shells. *Chem. Commun.* **2008**, 196–198.
29. Jewell, C. M.; Jung, J.-M.; Atukorale, P. U.; Carney, R. P.; Stellacci, F.; Irvine, D. J. Oligonucleotide Delivery by Cell-Penetrating "Striped" Nanoparticles. *Angew. Chem., Int. Ed.* **2011**, *50*, 12312–12315.
30. Verma, A.; Uzun, O.; Hu, Y.; Hu, Y.; Han, H.-S.; Watson, N.; Chen, S.; Irvine, D. J.; Stellacci, F. Surface-Structure-Regulated Cell-Membrane Penetration by Monolayer-Protected Nanoparticles. *Nat. Mater.* **2008**, *7*, 588–595.
31. Carney, R.; Carney, T.; Mueller, M.; Stellacci, F. Dynamic Cellular Uptake of Mixed-Monolayer Protected Nanoparticles. *Biointerphases* **2012**, *7*, 1–9.

32. Leduc, C.; Jung, J.-M.; Carney, R. R.; Stellacci, F.; Lounis, B. Direct Investigation of Intracellular Presence of Gold Nanoparticles *via* Photothermal Heterodyne Imaging. *ACS Nano* **2011**, *5*, 2587–2592.
33. Carney, R. P.; Astier, Y.; Carney, T. M.; Voïtchovsky, K.; Jacob Silva, P. H.; Stellacci, F. Electrical Method To Quantify Nanoparticle Interaction with Lipid Bilayers. *ACS Nano* **2013**, *7*, 932–942.
34. Andala, D. M.; Shin, S. H. R.; Lee, H.-Y.; Bishop, K. J. M. Templated Synthesis of Amphiphilic Nanoparticles at the Liquid−Liquid Interface. *ACS Nano* **2012**, *6*, 1044–1050.
35. Lee, H.-Y.; Shin, S. H. R.; Abezgauz, L. L.; Lewis, S. A.; Chirsan, A. M.; Danino, D. D.; Bishop, K. J. M. Integration of Gold Nanoparticles into Bilayer Structures *via* Adaptive Surface Chemistry. *J. Am. Chem. Soc.* **2013**, *135*, 5950–5953.
36. Hildebrand, J. H.; Prausnitz, J. M.; Scott, R. L. *Regular and Related Solutions: The Solubility of Gases, Liquids, and Solids*; Van Nostrand Reinhold: New York, 1970.
37. *CRC Handbook of Chemistry and Physics*, 88th ed.; CRC Press: Boca Raton, FL, 2007.
38. Vella, D.; Aussillous, P.; Mahadevan, L. Elasticity of an Interfacial Particle Raft. *Europhys. Lett.* **2004**, *68*, 212.
39. Vella, D.; Kim, H.-Y.; Aussillous, P.; Mahadevan, L. Dynamics of Surfactant-Driven Fracture of Particle Rafts. *Phys. Rev. Lett.* **2006**, *96*, 178301.
40. Shipway, A. N.; Katz, E.; Willner, I. Nanoparticle Arrays on Surfaces for Electronic, Optical, and Sensor Applications. *ChemPhysChem* **2000**, *1*, 18–52.
41. Puntes, V. F.; Gorostiza, P.; Aruguete, D. M.; Bastus, N. G.; Alivisatos, A. P. Collective Behaviour in Two-Dimensional Cobalt Nanoparticle Assemblies Observed by Magnetic Force Microscopy. *Nat. Mater.* **2004**, *3*, 263–268.
42. Majetich, S. A.; Wen, T.; Booth, R. A. Functional Magnetic Nanoparticle Assemblies: Formation, Collective Behavior, and Future Directions. *ACS Nano* **2011**, *5*, 6081–6084.
43. Chen, M.-C.; Yang, Y.-L.; Chen, S.-W.; Li, J.-H.; Aklilu, M.; Tai, Y. Self-Assembled Monolayer Immobilized Gold Nanoparticles for Plasmonic Effects in Small Molecule Organic Photovoltaic. *ACS Appl. Mater. Interfaces* **2013**, *5*, 511–517.
44. Zhou, Y.; Han, S.-T.; Xu, Z.-X.; Roy, V. A. L. Controlled Ambipolar Charge Transport through a Self-Assembled Gold Nanoparticle Monolayer. *Adv. Mater.* **2012**, *24*, 1247–1251.
45. Kim, S. I.; Pradal, F.; Song, H.; Kim, S. Formation of Single-Domain Homogeneous Au Nanoparticle Monolayer at the Water/Oil Interface and Its Application to Surface-Enhanced Raman Scattering. *J. Vac. Sci. Technol., B* **2011**, *29*, 021801.
46. Tien, J.; Terfort, A.; Whitesides, G. M. Microfabrication through Electrostatic Self-Assembly. *Langmuir* **1997**, *13*, 5349–5355.
47. Thebault, P.; Taffin de Givenchy, E.; Levy, R.; Vandenberghe, Y.; Guittard, F.; Géribaldi, S. Preparation and Antimicrobial Behaviour of Quaternary Ammonium Thiol Derivatives Able To Be Grafted on Metal Surfaces. *Eur. J. Med. Chem.* **2009**, *44*, 717–724.
48. Jana, N. R.; Peng, X. Single-Phase and Gram-Scale Routes toward Nearly Monodisperse Au and Other Noble Metal Nanocrystals. *J. Am. Chem. Soc.* **2003**, *125*, 14280–14281.